A 3-D Surface Reconstruction Approach Based on Postnonlinear ICA Model

Chin-Teng Lin, *Fellow, IEEE*, Wen-Chang Cheng, and Sheng-Fu Liang

***Abstract*—Photometric stereo technique deals with the reconstruction of three–dimensional (3-D) shape of an object by using several images of the same surface taken from the same viewpoint but under illuminations from different directions. In this paper, we propose a new photometric stereo scheme based on a new reflectance model and the postnonlinear (PNL) independent components analysis (ICA) method. The proposed nonlinear reflectance model consists of diffuse components and specular components for modeling the surface reflectance of a stereo object in an image. Unlike the previous approaches, these two components are not separated and processed individually in the proposed model. An unsupervised learning adaptation algorithm is developed to estimate the reflectance model based on image intensities. In this algorithm, the PNL ICA method is used to obtain the surface normal on each point of an image. Then, the 3-D surface model is reconstructed based on the estimated surface normal on each point of image by using the enforcing integrability method. Two experiments are performed to assess the performance of the proposed approach. We test our algorithm on synthetically generated images for the reconstruction of surface of objects and on a number of real images captured from the Yale Face Database B. These testing images contain variability due to illumination and varying albedo in each point of surface of human faces. All the experimental results are compared to those of the existing photometric stereo approaches tested on the same images. The results clearly indicate the superiority of the proposed nonlinear reflectance model over the conventional Lambertian model and the other linear hybrid reflectance model.**

***Index Terms*—Enforcing integrability, Lambertian model, neural network, photometric stereo, reflectance model, surface normal.**

I. Introduction

DETERMINING the shape of objects from an image in a scene is extremely difficult. The image typically exhibits a smooth variation in brightness from one point to another, which is known as shading. This perception of shape from gradual changes in brightness is denoted as *shape from shading* (SfS). It was one of the first areas of study in computer vision and was proposed by Horn [1] in the early 1970s. Unfortunately, measurements of brightness at a single point in the image only provide one constraint, whereas describing surface orientation requires two variables. Therefore, it is an ill-posed problem. In addition, the method must have knowledge of the reflectance properties of the surface.

Photometric stereo approach is able to estimate local surface orientation by using several images of the same surface taken from the same viewpoint but under illuminations from different directions. It was first introduced based on the Lambertian reflectance model by Woodham [2]. It has received wide attention and several efforts have been made to improve the performance of recovery [3]–[21]. The main limitation of classical photometric stereo approach is that the light source positions must be accurately known and this necessitates a fixed, calibrated lighting rig. Hence, an improved photometric stereo method for estimating the surface normal and the surface reflectance of objects without a priori knowledge of the light source direction or the light source intensity is proposed by Hayakawa [20]. The method used the singular-value decomposition (SVD) method to factorize image data matrix of three different illuminations into surface reflectance matrix and light source matrix based on the Lambertian model. However, they still used one of the two added constraints (i.e., at least 6 pixels in which relative value of the surface reflection is constant or known and at least 6 frames in which the relative value of the light-source intensity is constant or known) for finding the linear transformation between the surface reflectance matrix and the light source matrix. McGunnigle [7] introduced a simple photometric stereo scheme which only considered a Lambertian reflectance model, where the self and cast shadow as well as inter-reflections were ignored. Three images at tilt angle of 90° increments were captured. He suggested using his method as a first estimate for an iterative procedure. In fact, this method is a simplified version of Woodham's method in which the illumination directions are chosen by mathematics simplification. Belhumeur, etc. [10] showed that a generalized bas-relief transformation is a transformation of both the surface shape and the surface albedo for an arbitrary Lambertian surface. The set of images of an object in fixed post but under all possible illumination conditions is a convex cone (illumination cone) in the space of images. When the surface reflectance can be approximated as Lambertian, this illumination cone can be constructed from a handful of images acquired under variable lighting. They used as few as seven images of a face seen in a fixed pose, but illumination by point light sources at varying, unknown position, to estimate its surface geometry and albedo map up to a generalized bas-relief transformation. Despite they announced their success under unknown light source directions,

Manuscript received April 12, 2004; revised April 28, 2005. This work was supported in part by the Ministry of Education, Taiwan, by Grant EX-91-E-FA06-4-4 and by the Ministry of Economic Affairs, Taiwan, by Grant 94-EC-17-A-02-S1-032.

C.-T. Lin is with the Department of Electrical and Control Engineering and the Department of Computer Science, National Chiao-Tung University, Hsinchu, Taiwan. He is also with the Brain Research Center, University System of Taiwan, Taipei, Taiwan (e-mail: ctlin@mail.nctu.edu.tw).

S.-F. Liang is with the Department of Biological Science and Technology, National Chiao-Tung University, Hsinchu, Taiwan. He is also with the Brain Research Center, University System of Taiwan, Taipei, Taiwan (e-mail: sfliang@mail.nctu.edu.tw).

W.-C. Cheng is with the Department of Information Networking Technology, Hsiuping institute of Technology, Taichung, Taiwan (e-mail: wccheng@mail.hit.edu.tw).

Digital Object Identifier 10.1109/TNN.2005.857950

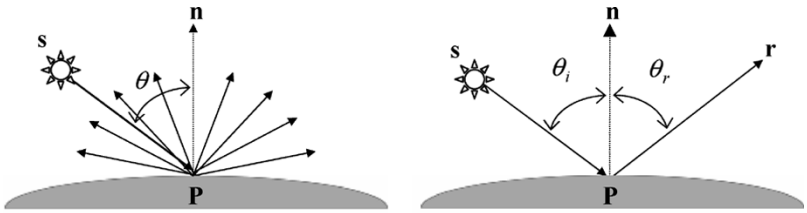

Fig. 1. Illustration of diffuse reflection. $\mathbf{s}$ is a point light source, $\mathbf{n}$ is the normal vector of surface on point $\mathbf{P}$, θ is the angle between light source and the normal. The diffuse reflection scatters incoming light equally in all directions. (b) Illustration of specular reflection. It obeys Shell's law, that is, $\theta_i = \theta_r$.

the estimation of surface methods still need to be assisted with some added constraints or more images.

Another more difficult problem is estimating a surface with an unknown reflectance map. Cho and Minamitani [4] tried to reduce three–dimensional (3-D) reconstruction errors due to specularities. Since the specular reflection produced incorrect surface normal by elevating the image intensity, they readjusted the pixel with greatest intensity by re-scaling with a modified reflectivity. Kay and Caelli [6] used the photometric stereo method to estimate not only the surface normal but also the roughness parameters associated with the Torrance-Sparrow (TS) reflectance model. The basis they used was to apply nonlinear regression techniques to the photometric stereo method. Nayar [8] used a linear combination of Lambertian and an impulse specular component. He used distributed light sources for photometric stereo of surface whose reflection is a linear sum of specular and Lambertian components.

In this paper, we propose a novel postnonlinear (PNL) ICA-based reflection model that consists of the diffuse components and the specular components. We do not need to separate the two components from the novel nonlinear reflection model. An unsupervised learning adaptation algorithm is used to tune up the proportion of hybrid automatically based on image intensities. The technique of the PNL independent components analysis (ICA) [22], [23] is used to solve the surface normal on each point of an image. The goal of PNL ICA is to nonlinearly transform the data such that the transformed variables are as statistically independent from each other as possible. Finally, the 3-D surface model is reconstructed from the surface normal on each point of an image, obtained by the PNL ICA technique, using the method of enforcing integrability [24]. The reason is that it is easy to implement.

The rest of this paper is organized as follows. Section II describes the basic reflectance models, including the Lambertian model and non-Lambertian. The details of the proposed PNL ICA-based reflectance model and its derivations are presented in Section III. Extensive experiments have been performed to evaluate the performance of the proposed approach, and parts of the results are presented in Section VI. Conclusions are summarized in the last section.

II. The Basic Reflectance Models

There are mainly two kinds of light reflection components considered in computer vision: diffuse reflection and specular reflection. Diffuse reflection is a uniform reflection of light with no directional dependence for the viewer. The phenomenon of diffuse reflection is illustrated in Fig. 1(a). $\mathbf{s}$ is a point light source, $\mathbf{n}$ is the normal vector of the surface on point P, θ is the angle between light source direction and the normal vector of the surface. When $\mathbf{s}$ illuminates straightly to the surface, the diffuse reflection scatters incoming light equally in all directions. Thus we have identical reflected energy for all viewing directions. The light reaching the surface is reflected in the reflected direction with the same angle. The phenomenon of specular reflection is illustrated in Fig. 1(b). It means if a point light source $\mathbf{s}$ illuminates to the surface, the reflected light is visible only at the reflected direction $\mathbf{r}$, where $\theta_i = \theta_r$.

It is important that a good reflectance model should be able to describe the surface shape accurately from the image intensity [8]. Basically, the reflectance surface can be categorized to be Lambertian or non-Lambertian. The Lambertian surfaces are surfaces that only have diffuse reflectance, which implies that the surface reflects light equally in all direction. On the other hand, the non-Lambertian model considers the specular component in addition to the diffuse component in the Lambertian model.

A. Lambertian Model

Suppose that the recovering of surface shape, denoted by $z(x, y)$, from shaded images depends upon the systematic variation of image brightness with surface orientation, where z is the depth field, and x and y form the 2-D grid over the domain D of the image plane. Then, the Lambertian reflectance model used to represent a surface illuminated by a single point light source is written as

$$R_d\left(\mathbf{n}(x,y), \alpha(x,y)\right) = L\alpha(x,y)\mathbf{s}^T\mathbf{n}(x,y),\ \forall x, y \in D \quad (1)$$

where $R_d(\cdot)$ is diffuse component intensity, $\alpha(x, y)$ is diffuse albedo on position (x, y) of surface, $\mathbf{s}$ is a column vector indicating the direction of point light, and L is light strength. The surface normal on position (x, y), denoted by $\mathbf{n}(x, y)$, can be represented as

$$\mathbf{n}(x,y) = \frac{\begin{bmatrix}-p(x,y) & -q(x,y) & 1\end{bmatrix}^T}{\sqrt{p^2(x,y)+q^2(x,y)+1}} \quad (2)$$

where $p(x,y) = \partial z(x,y)/\partial x$ and $q(x,y) = \partial z(x,y)/\partial y$ are the surface gradients [2].

The Lambertian model describes a simple nonshiny surface where any incident light is reflected evenly in all directions after modulation by the surface's reflectivity. It is a simple but useful reflectance model. It is commonly adopted in the field of computer vision as a model of the ideal surface. Despite the simplicity and the popularity of the Lambertian model, it is quite

well known that this model is unable to generalize with strong specular components. However, in most cases, the reflectance of objects does not always follow the Lambertian model. Considering only the diffuse component is not enough for practical applications, so a more general non-Lambertian reflectance model is required.

B. Non-Lambertian Model

In order to effectively exhibit the reflectance model, both the diffuse component and specular component should be considered for reconstructing the surfaces of 3-D objects. The kind of hybrid model is called non-Lambertian model. Specular component occurs when the incident angle of the light source is equal to the reflected angle and this component is formed by two terms: the specular spike and the lobe. The specular spike is zero in all directions except for very narrow range around the directions of specular reflectance. The specular lobe spreads around the direction of specular reflectance. The specular components used to represent a surface illuminated by a single point light source is written as:

$$R_s\left(\mathbf{n}(x,y),\beta(x,y)\right) = L\beta(x,y)\left(\mathbf{h}^T\mathbf{n}(x,y)\right)^m,\ \forall x,y \in D \tag{3}$$

where $R_s(\cdot)$ is specular component intensity, $\beta(x,y)$ is specular albedo on position (x,y) of surface, and the vector $\mathbf{h} = (\mathbf{s}+\mathbf{v})/\|\mathbf{s}+\mathbf{v}\|$ is usually called the halfway-vector and represents the normalized vector sum between the light source direction $\mathbf{s}$ and the viewing direction $\mathbf{v}$. With the specular component described in (3), the non-Lambertian model proposed in [8] can be represented as following linear combination equation

$$R_{hybrid}(x,y) = \lambda R_d(x,y) + (1-\lambda)R_s(x,y),\ \forall x,y \in D \tag{4}$$

where R_{hybrid} is the total intensity of the hybrid surface, and R_d and R_s are the diffuse intensity and the specular intensity, respectively, and λ is the weight of the diffuse component. However, the existing approach considers only the linear hybrid combination as described by (4). It is not enough to model a nonlinear hybrid reflectance model. Therefore, in this paper, we propose a novel nonlinear reflection model that consists of the diffuse components and the specular components. We do not need to separate the two components from this novel nonlinear reflection model, because an unsupervised learning adaptation algorithm based on images intensities can help to tune up the proportion of hybrid. In the next section, we shall give more discussions in the novel nonlinear reflection model.

C. The Proposed Nonlinear Reflectance Model

In this paper, we propose a new nonlinear reflectance model; it can model both the diffuse components and specular components into a single model. This model is described by

$$R_{\text{nonlinear}}\left(\mathbf{n}(x,y),\sigma(x,y),\gamma(x,y)\right) = L\gamma(x,y)\exp\left(-\frac{\left(\cos^{-1}\left(\mathbf{a}^T\mathbf{n}(x,y)\right)\right)^2}{2\sigma^2(x,y)}\right) \tag{5}$$

where $R_{\text{nonlinear}}(\cdot)$ denotes the nonlinear reflectance intensities, $\mathbf{a}$ is a 3×1 column vector and it represents to the light direction and viewing direction, L is light strength, and $\gamma(x,y)$ is composite albedo on position (x,y) of surface. $\sigma(x,y)$ is the variance of exponential function. Fig. 2 shows the normalized exponential functions with different sigma values, where angle is from $-\pi/2$ to $\pi/2$. When $\sigma(x,y)$ is large, the $R_{\text{nonlinear}}(\cdot)$ models more the diffuse component intensity. When $\sigma(x,y)$ gets smaller, $R_{\text{nonlinear}}(\cdot)$ models more the specular component intensity. So, we can obtain the best approximation by the adjustment of $\sigma(x,y)$. However, the following task is to solve the surface normal, $\mathbf{n}(x,y)$ for all x and y, of (5) from 2-D intensities images. Since the $\mathbf{n}(x,y)$ vector is a 3×1 column vector, it is a limit that we need at least three images under different light directions. If the location of light sources were given, we could solve the normal vector on surfaces of every location (x,y). But unfortunately, light sources could not be known in the general applications. Because the problem of solving (5) is a blind source separation problem [25]–[33], an unsupervised learning adaptation algorithm based on images intensities can be used in solving (5). The technique of the PNL ICA is used to solve the surface normal on each point of image. The PNL ICA is a technique that exploits higher-order statistical structure in data. The goal of PNL ICA is to nonlinearly transform the data such that the transformed variables are as statistically independent from each other as possible. The detail for how to find $\mathbf{n}(x,y)$ of each point in image is showed in the following PNL ICA model.

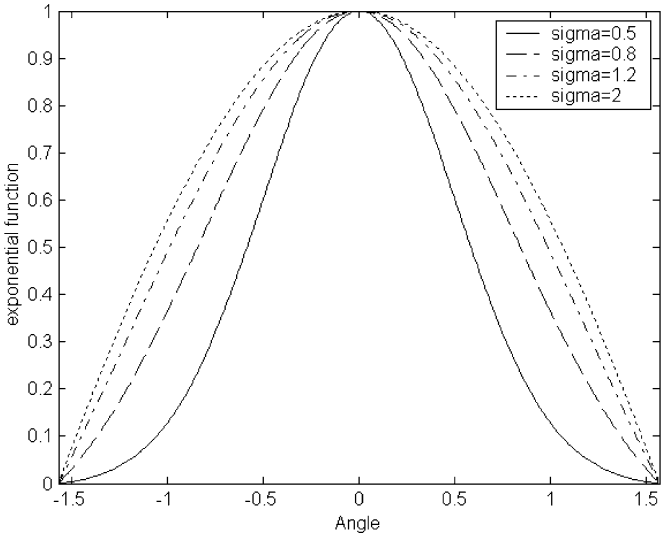

Fig. 2. Normalized exponential functions with different sigma values (Angle: $-(\pi/2) \sim (\pi/2)$.

III. Determining the Surface Normal of Objects by PNL ICA Model

In this section, we shall introduce the PNL ICA model and explain how to use this model to solve the normal vectors on surfaces of the objects in an image based on the nonlinear reflectance model that we proposed.

A. PNL ICA Model

In this section, we introduce the particular nonlinear mixtures, which can be considered to be a hybrid structure consisting of a linear stage followed by a nonlinear

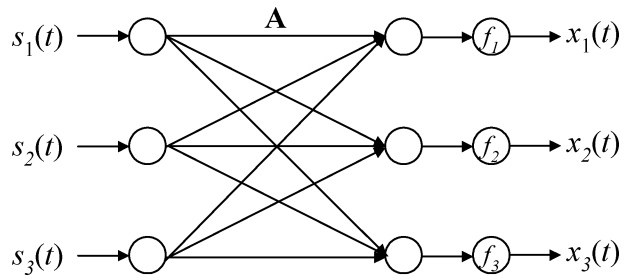

Fig. 3. PNL mixing ICA model ($n = 3$).

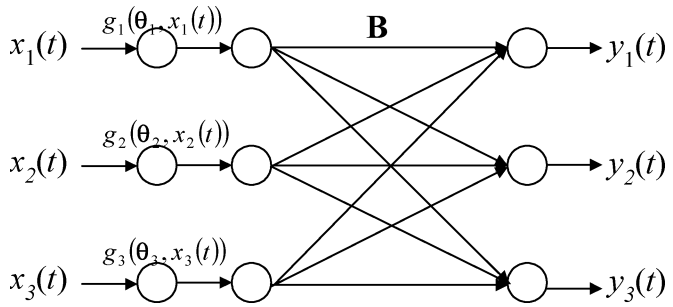

Fig. 4. Separation architecture of the PNL ICA model ($n = 3$).

stage. It is shown in Fig. 3. This structure, which was introduced by Taleb and Jutten [23], provides the observation $\mathbf{x}(t) = (x_1(t), x_2(t), \ldots, x_n(t))^T$, which is the unknown nonlinear mixture of the unknown statistically independent source $\mathbf{s}(t) = (s_1(t), s_2(t), \ldots, s_n(t))^T$

$$x_i(t) = f_i\left(\sum_{j=1}^{n} a_{ij} s_j(t)\right), \quad i = 1, 2, \ldots, n \tag{6}$$

where $f_i(\cdot)$ are unknown invertible derivable nonlinear functions, and $a_{ij} (i, j = 1, 2, \ldots, n)$ denote the scalar elements of a regular mixing matrix $\mathbf{A}$. In the following, the mixture vector $\mathbf{x}(t)$, and by extension the pair ($\mathbf{A}$, $\mathbf{f}$), will be called a PNL model.

Contrary to general nonlinear mixtures, the PNL model has a favorable separability property. That is, using the separation structure ($\mathbf{g}$, $\mathbf{B}$) shown in Fig. 4, it can be demonstrated, under weak conditions on the mixing matrix $\mathbf{A}$ and on the source distribution, that the output independence can be obtained if and only if $f_i \bullet g_i$ are linear for all index i from 1 to n. This means that the sources $\mathbf{y}(t) = (y_1(t), y_2(t), \ldots, y_n(t))^T$, which was estimated using an independence criterion on the outputs, are equal to the unknown sources with the same indeterminacies noted in linear mixture model.

B. PNL ICA Model by Maximum Likelihood (ML) Estimation

A very popular approach to estimating the ICA model is the ML estimation. ML estimation is a fundamental method of statistical estimation. One interpretation of ML estimation is that we take those parameter values as estimates that give the highest probability for the observations. In following section, we show how to apply ML estimation technique to PNL ICA estimation. The similar derivations of (7)–(17) based on the mutual information as a cost function are shown in the paper by Taleb [22], [23].

1) Independence Criterion and Deriving the Likelihood: The statistical independence of the sources is the main assumption. Then, any separation architecture is tuned so that the components of its output y become statistically independent. This is achieved if the joint density factorizes as the product of the marginal densities

$$p(\mathbf{y}) = \prod_{i=1}^{n} p_i(y_i). \tag{7}$$

According to this result, the density $p_x(\mathbf{x})$ of the mixture vector $\mathbf{x} = \mathbf{f}(\mathbf{A}\mathbf{s})$ can be formulated as

$$\begin{aligned} p_x(\mathbf{x}) &= |\det \mathbf{B}| \prod_{i=1}^{n} |g'(\theta_i, x_i)|\, p(\mathbf{y}) \\ &= |\det \mathbf{B}| \prod_{i=1}^{n} |g'(\theta_i, x_i)| \prod_{j=1}^{n} p_j(y_j) \end{aligned} \tag{8}$$

where $\mathbf{B} = \mathbf{A}^{-1}$, $g(\cdot)$ is the inverse function of $f(\cdot)$, the parameters $\boldsymbol{\theta}_i$ are adjusted to cancel the effect of nonlinear function $f(\cdot)$, and the $p_j(y_j)$ denote the densities of the independent components. Equation (8) can be expressed as a function of $\mathbf{B} = (\mathbf{b}_1, \mathbf{b}_2, \ldots, \mathbf{b}_n)^T$ and $\mathbf{x}$, giving

$$p_x(\mathbf{x}) = |\det \mathbf{B}| \prod_{i=1}^{n} |g'(\boldsymbol{\theta}_i, x_i)| \prod_{j=1}^{n} p_j\left(\mathbf{b}_j^T \mathbf{g}(\boldsymbol{\theta}, \mathbf{x})\right) \tag{9}$$

where $\mathbf{g}(\boldsymbol{\theta}, \mathbf{x}) = (g_1(\boldsymbol{\theta}_1, x_1), g_2(\boldsymbol{\theta}_2, x_2), \ldots, g_n(\boldsymbol{\theta}_n, x_n))^T$.

Assume that we have T observations of $\mathbf{x}$, denoted by $\mathbf{x}(1)$, $\mathbf{x}(2), \ldots, \mathbf{x}(t), \ldots, \mathbf{x}(T)$. Then the likelihood can be obtained as the product of this density evaluated at the T points. This is denoted by $L(\mathbf{B}, \boldsymbol{\theta})$ and we have

$$L(\mathbf{B}, \boldsymbol{\theta}) = \prod_{t=1}^{T} |\det \mathbf{B}| \prod_{i=1}^{n} |g'(\boldsymbol{\theta}_i, x_i)| \prod_{j=1}^{n} p_j\left(\mathbf{b}_j^T \mathbf{g}\left(\boldsymbol{\theta}, \mathbf{x}(t)\right)\right). \tag{10}$$

In general, it is more practical to use the logarithm of the likelihood, since it is algebraically simpler. This does not make any difference here since the maximum of the logarithm is obtained at the same point as the maximum of the likelihood. The log-likelihood is given by

$$\begin{aligned} &\log L(\mathbf{B}, \boldsymbol{\theta}) \\ &\quad = \sum_{t=1}^{T} \log\left\{ \prod_{i=1}^{n} |g'(\boldsymbol{\theta}_i, x_i)| \prod_{j=1}^{n} p_j\left(\mathbf{b}_j^T \mathbf{g}\left(\boldsymbol{\theta}, \mathbf{x}(t)\right)\right) |\det \mathbf{B}| \right\} \\ &\quad = \sum_{t=1}^{T} \left\{ \sum_{i=1}^{n} \log |g'(\boldsymbol{\theta}_i, x_i)| \right. \\ &\qquad \left. + \sum_{j=1}^{n} \log\left[p_j\left(\mathbf{b}_j^T \mathbf{g}\left(\boldsymbol{\theta}, \mathbf{x}(t)\right)\right)\right] + \log |\det \mathbf{B}| \right\}. \end{aligned} \tag{11}$$

To simplify notation and to make it consistent to what can denote the sum over the sample index t by an expectation operator, thus, we have

$$\frac{1}{T}\log L(\mathbf{B},\boldsymbol{\theta}) = E\left\{\sum_{i=1}^{n}\log|g'(\boldsymbol{\theta}_i,x_i)|\right\} + E\left\{\sum_{j=1}^{n}\log\left[p_j\left(\mathbf{b}_j^T\mathbf{g}\left(\boldsymbol{\theta},\mathbf{x}(t)\right)\right)\right]\right\} + \log|\det\mathbf{B}| \quad (12)$$

where the expectation operator here is an average computed from the observed samples.

2) The Derivation of Adaptation Rules With ML Estimation: To perform maximum log-likelihood estimation in practice, we need an algorithm to perform the numerical maximization of log-likelihood. In this section, we perform the numerical maximization of log-likelihood by gradient methods. First, the maximization of the log-likelihood requires the computation of its gradient with respect to the separation architecture parameters $\mathbf{B}$ and $\boldsymbol{\theta}_i$, $i = 1, 2, \ldots, n$.

The first layer: To estimate the linear stage parameters, we must compute the gradient of log-likelihood of (12) with respect to the separation architecture parameters $\mathbf{B}$. Therefore, we have

$$\frac{1}{T}\frac{\partial\log L(\mathbf{B},\boldsymbol{\theta})}{\partial\mathbf{B}} = E\left\{\sum_{j=1}^{n}h_j\left(\mathbf{b}_j^T\mathbf{g}\left(\boldsymbol{\theta},\mathbf{x}(t)\right)\right)\mathbf{g}\left(\boldsymbol{\theta},\mathbf{x}(t)\right)^T\right\} + \left(\mathbf{B}^T\right)^{-1} \quad (13)$$

where

$$h_j(y_j) = \frac{\partial\log p_{y_j}(y_j)}{\partial y_j} = \frac{p'_{y_j}(y_j)}{p_{y_j}(y_j)} \text{ and } y_j = \mathbf{b}_j^T\mathbf{g}\left(\boldsymbol{\theta},\mathbf{x}(t)\right).$$

Therefore, this immediately gives the following adaptation rule for ML estimation

$$\Delta\mathbf{B} \propto E\left\{\sum_{j=1}^{n}h_j\left(\mathbf{b}_j^T\mathbf{g}\left(\boldsymbol{\theta},\mathbf{x}(t)\right)\right)\mathbf{g}\left(\boldsymbol{\theta},\mathbf{x}(t)\right)^T\right\} + \left(\mathbf{B}^T\right)^{-1} \quad \text{and} \quad (14)$$

$$\mathbf{B}^{(k+1)} = \mathbf{B}^{(k)} + \eta_{\mathbf{B}}(\Delta\mathbf{B}) \quad (15)$$

where $\eta_{\mathbf{B}}$ is the learning rate for adapting $\mathbf{B}$. This result has the same expression as in the linear source separation. This algorithm is often called the Bell-Sejnowski algorithm [25]. It is the simplest algorithm for maximizing likelihood by gradient methods. However, due to the inversion of the matrix $\mathbf{B}$ in (14) is needed in every step, it converges very slowly. The convergence can be improved by whitening the data, and especially by using the natural gradient [26] that is based on the geometrical structure of the parameter space. Therefore, (16) is used to estimate the linear stage instead of (14).

$$\Delta\mathbf{B} \propto \left(E\left\{\sum_{j=1}^{n}h_j\left(\mathbf{y}(t)\right)\mathbf{y}(t)^T\right\} + \mathbf{I}\right)\mathbf{B} \quad (16)$$

where $\mathbf{y}(t) = \mathbf{b}_j^T\mathbf{g}(\boldsymbol{\theta},\mathbf{x}(t))$.

The second layer: The derivation of the log-likelihood with respect to parameters $\boldsymbol{\theta}_i$ of the nonlinear function $g_i(\boldsymbol{\theta}_i, x_i)$ is

$$\frac{1}{T}\frac{\partial\log L(\mathbf{B},\boldsymbol{\theta})}{\partial\boldsymbol{\theta}_i} = E\left\{\frac{\partial\log|g'_i(\boldsymbol{\theta}_i,x_i)|}{\partial\boldsymbol{\theta}_i}\right\} + E\left\{\left[\sum_{j=1}^{n}h_j\left(\mathbf{b}_j^T\mathbf{g}\left(\boldsymbol{\theta},\mathbf{x}(t)\right)\right)b_{ji}\right]\frac{\partial g_i(\boldsymbol{\theta}_i,x_i)}{\partial\boldsymbol{\theta}_i}\right\}. \quad (17)$$

From the derivation of the log-likelihood with respect to parameters $\boldsymbol{\theta}_i$, we update the parameters $\boldsymbol{\theta}_i$ of the $g_i(\boldsymbol{\theta}_i, \mathbf{x}(t))$ function by the following adaptation rule

$$\Delta\boldsymbol{\theta}_i \propto E\left\{\frac{\partial\log|g'_i(\boldsymbol{\theta}_i,x_i)|}{\partial\boldsymbol{\theta}_i}\right\} + E\left\{\left[\sum_{j=1}^{n}h_j\left(\mathbf{b}_j^T\mathbf{g}\left(\boldsymbol{\theta},\mathbf{x}(t)\right)\right)b_{ji}\right]\times\frac{\partial g_i(\boldsymbol{\theta}_i,x_i)}{\partial\boldsymbol{\theta}_i}\right\} \text{ and} \quad (18)$$

$$\boldsymbol{\theta}_i^{(k+1)} = \boldsymbol{\theta}_i^{(k)} + \eta_{\boldsymbol{\theta}_i}(\Delta\boldsymbol{\theta}_i) \quad (19)$$

where $\eta_{\boldsymbol{\theta}_i}$ is the learning rate of adapting $\boldsymbol{\theta}_i$.

3) Estimation of the Source Densities: Denoted by $p_{\mathbf{y}}(\mathbf{y})$ the assumed densities of the independent components, and

$$h_j(y_j) = \frac{\partial\log p_{y_j}(y_j)}{\partial y_j} = \frac{p'_{y_j}(y_j)}{p_{y_j}(y_j)}. \quad (20)$$

Constrain the estimates of independent components $y_j = \mathbf{b}_j^T\mathbf{g}(\boldsymbol{\theta},\mathbf{x}(t))$ to be uncorrelated and to have unit variance. Then the ML estimator is locally consistent, if the assumed densities $p_{y_j}(y_j)$ fulfill

$$E\left\{y_j h_j(y_j) - h'_j(y_j)\right\} > 0,\ \forall j. \quad (21)$$

The proof can be found in the [27]. Therefore, the limitation shows how to construct families consisting of only two densities, so that the condition in (21) is true for one of these densities. For example, consider the following log-densities

$$\log p^+(s) = \alpha_1 - 2\log\cosh(s) \quad (22)$$

$$\log p^-(s) = \alpha_2 - \left(\frac{s^2}{2} - \log\cosh(s)\right) \quad (23)$$

where α_1, α_2 are positive parameters that are fixed so as to make these two functions logarithms of probability densities. Actually, these constants can be ignored in the following. Then, for super-Gaussian independent components, the pdf defined by (22) is usually used. This means that the nonlinear function $h(\cdot)$ is the tanh function

$$h^+(y) = -2\tanh(y). \quad (24)$$

For sub-Gaussian independent components, the other pdf defined by (23) is used. Then the nonlinear function $h(\cdot)$ can be written as

$$h^-(y) = \tanh(y) - y. \quad (25)$$

Finally, the choice between the two nonlinearities in (24) and (25) can be made by computing the nonpolynomial moment

$$k_j = sign\left\{E\left[-\tanh(y_j)y_j + \left(1-\tanh(y_j)^2\right)\right]\right\} \quad j = 1, 2, \ldots, n \quad (26)$$

using some estimates of the independent components. Then, the source distribution is super-Gaussian when $k_j = 1$ and sub-Gaussian when $k_j = -1$, where the expectation value in the formulas is for all t, $t = 1, 2, \ldots, T$.

C. Solving the Proposed Nonlinear Reflectance Model by PNL ICA Model

In this section, we shall describe the way of applying the PNL ICA model to estimate the normal vector $\mathbf{n}(x, y)$ on the object surface corresponding to each pixel in the image. Since the $\mathbf{n}(x, y)$ vector is a 3×1 column vector, it is required that we need at least three images under different light directions for its estimation. Hence, to reconstruct the 3-D surface of an object through its images, we have to take three gray-value images under three different illuminants. Assuming an image contains T pixels in total, then we can rearrange all the gray values of the three images into a $3 \times T$ matrix, with each row representing an image, and each column the gray values of a single pixel under three different illuminants. Putting this matrix into (5), and comparing (5) with (6), we can define the nonlinear function in the PNL ICA model as

$$f_j\left(o_j(t)\right) = L\gamma(t)\exp\left(-\frac{\left(\cos^{-1}\left(o_j(t)\right)\right)^2}{2\sigma^2(t)}\right) \quad t = 1, 2, \ldots, T, \text{ and } j = 1, 2, 3 \quad (27)$$

where $o(t) = \sum_{i=1}^{3} a_i s_i(t)$ and $\mathbf{s}(t)$ is the $\mathbf{n}(x, y)$ vector that we are looking for. From (27), we can obtain the inverse nonlinear $f(\cdot)$ function as

$$g_j\left(\sigma(t), I_j(t)\right) = \cos\left(\sqrt{-2\sigma^2(t)\ln\left(\frac{I_j(t)}{\gamma(t)}\right)}\right) \quad t = 1, 2, \ldots, T, \text{ and } j = 1, 2, 3 \quad (28)$$

where $\mathbf{I}(t)$ is the input vector, i.e., the three gray values of the tth pixel of the three images with different illuminants, and $\sigma(t)$ is the variant of the tth pixel in the exp() function in (27). We shall feed the input vectors, $\mathbf{I}(t)$, $t = 1, 2, \ldots, T$, to the input of the network shown in Fig. 4. Because all these input vectors come from the images belonging to the same object, the estimated reflectance model should be exactly the same for each of the three images; i.e., all the $g_i(\cdot)$, $i = 1, 2, 3$ are the same. With such setting, we can obtain the final outputs through the network computations shown in Fig. 4. To ensure the final outputs to be independent components, we apply the unsupervised adaptation rules derived in Section III-B-2 to tune $\sigma(t)$ and $\mathbf{B}$ matrix. Upon convergence, the final output is the estimated normal vector $\mathbf{n}(x, y)$ on the object surface corresponding to the tth pixel in the image for $t = 1, 2, \ldots, T$. The complete algorithm for the above computation is shown in Fig. 5, which consists of 9 steps.

Algorithm:

1. Set $k = 1$ and arbitrarily assign the initial values of $\sigma(t)$ and $\gamma(t)$, $t = 1, \ldots, T$, and $\mathbf{B}_\circ$
2. Set sampling index $t = 1$.
3. Compute $\mathbf{e}(t)$ from Eq. (27),
$$e_i(t) = \cos\left(\sqrt{-2\sigma^2(t)\ln\left(I_i(t)/\gamma(t)\right)}\right), \quad i = 1, 2, 3.$$
4. Compute $\mathbf{y}(t)$ as follows:
$$\mathbf{y}(t) = \mathbf{B}\mathbf{e}(t).$$
5. Calculate the normal vector of surface $\mathbf{n}(t) = \dfrac{\mathbf{y}(t)}{\|\mathbf{y}(t)\|}$ and the surface albedo $\gamma(t) = \|\mathbf{y}(t)\|$, $\forall t$.
6. Update $\mathbf{B}$ matrix by
$$\mathbf{B}^{(k+1)} = \mathbf{B}^{(k)} + \eta_{\mathbf{B}}\left\{\mathbf{I} + \left[\mathbf{h}\left(\mathbf{y}(t)\right)\mathbf{y}(t)^T\right]\right\}\mathbf{B}^{(k)},$$
where $\eta_{\mathbf{B}}$ is the learning rate of $\mathbf{B}$.
7. Update $\sigma(t)$ value using the following equation:
$$\sigma_i(t)^{(k+1)} = \sigma_i(t)^{(k)} + \eta_\sigma\left\{\frac{2}{\sigma_i(t)} + 4\sigma_i(t)\log\left(x_i(t)\right)\left[\sum_{j=1}^{3} h_j\left(y_j\right)b_{ji}\right]\right\},$$
where η_σ is the learning rate of σ.
8. Repeat Step 3~Step 7, until t equal to T.
9. Set $k = k + 1$ and repeat Step 2~Step 8, until convergence.

Fig. 5. Unsupervised updating rules for the proposed 3-D surface reconstruction scheme.

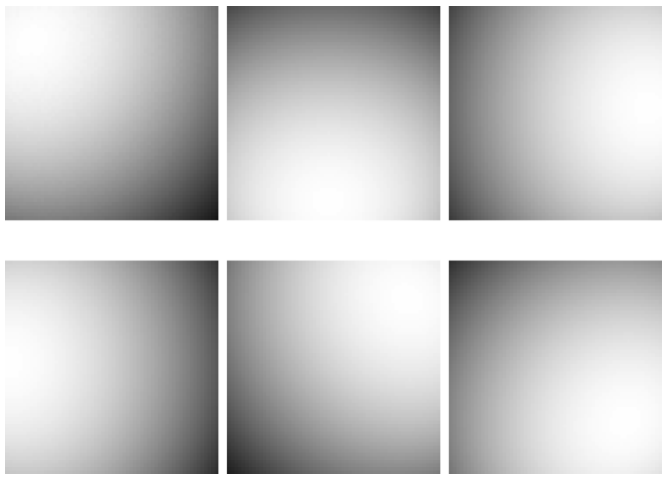

Fig. 6. Shadow images of sphere object with different light directions.

The separation architecture of the PNL ICA model can be considered to be a hybrid structure consisting of a nonlinear stage followed by a linear stage. Therefore, after compensating for the postnonlinearities, the problem is essentially reduced to a linear mixture of the form [matrix depending on lighting and viewing directions] $*$ [surface normal vector]. Using the ICA decomposition, we rewrite the equation in Step 4 in Fig. 5 as

$$\mathbf{y}(t) = \mathbf{B}\mathbf{e}(t), \text{ or } \mathbf{e}(t) = \mathbf{B}^{-1}\mathbf{y}(t) = \gamma(t)\hat{\mathbf{A}}^T\hat{\mathbf{n}}(t) \quad (29)$$

where $\hat{\mathbf{A}}^T = [\mathbf{a}_1, \mathbf{a}_2, \mathbf{a}_3]^T = \mathbf{B}^{-1}$ is the matrix depending on lighting and viewing directions and has unit length, $\hat{\mathbf{n}}(t)$ is the estimated normal vector corresponding to the tth pixel, $t = 1, 2, \ldots, T$, and $\gamma(t)$ is albedo of the tth pixel. However, the

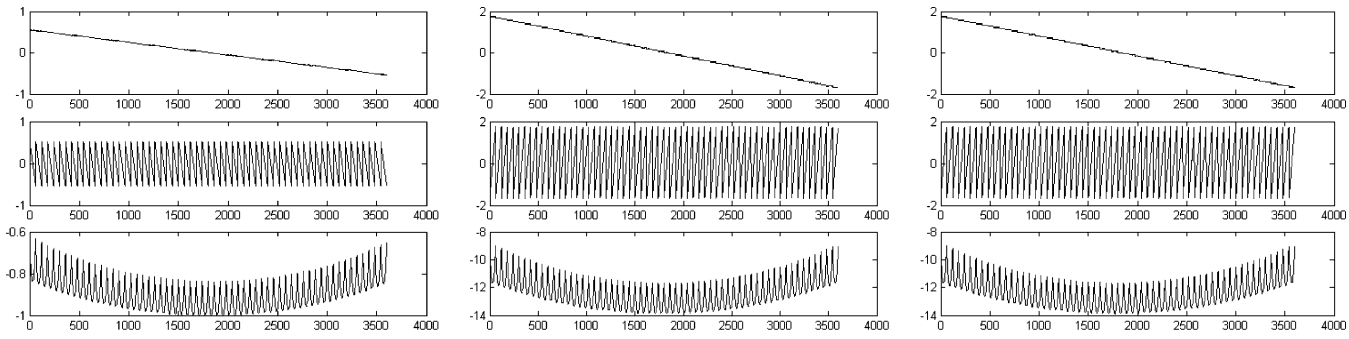

Fig. 7. The estimated normal vectors of sphere object by our approach. (a) The true normal vectors. (b) The estimated normal vectors from the first row of Fig. 5. (c) The estimated normal vectors from the second row of Fig. 5.

decomposition in (29) is not unique. If there is an invertible matrix $\mathbf{G}$, which satisfies

$$\mathbf{A}^T = \hat{\mathbf{A}}^T\mathbf{G} \quad \text{and} \quad \mathbf{n} = \mathbf{G}^{-1}\hat{\mathbf{n}} \tag{30}$$

where $\mathbf{A}$ and $\mathbf{n}(t)$ are, respectively, the true matrix depending on lighting and viewing directions of images $\mathbf{I}$, and the normal vector of the tth pixel in the standard XYZ coordinates, then the linear ambiguity is belonging to a generalized bas-relief (GBR) [10]–[12] transformation. A GBR transformation scales the surface and introduces an additive plane. There is an inherent nine-parameter ambiguity in the surface normals, light source and viewing directions of images. According to Georghiades's [12] studies, if the surface of an object is seen under variable light direction, but with fixed viewpoint, then the linear ambiguity can be reduced to three GBR parameters. As far as the surface normal vectors are concerned, we can only recover

$$\mathbf{n} \cong \mathbf{G}^{-1}\hat{\mathbf{n}}$$

and

$$\mathbf{G}^{-1} = \frac{1}{g_3}\begin{bmatrix} g_3 & 0 & 0 \\ 0 & g_3 & 0 \\ -g_1 & -g_2 & 1 \end{bmatrix} \tag{31}$$

where g_i are the three GBR parameters. On the other hand, the three light sources corresponding to the three images do not lie in the same plane (noncoplanar), so the columns of matrix $\mathbf{A}$ are linearly independent. In addition, using the ICA decomposition in (29), we can obtain an independent basis matrix $\hat{\mathbf{A}}$, so the ambiguity can further be denoted a diagonal matrix, i.e., $g_1 = 0$ and $g_2 = 0$. So, the relation between the normals in the standard XYZ coordinates and those in the most independent coordinates system is only by g3 factor. For the performance evaluation of 3-D image reconstruction, both estimated surface and synthetic one are normalized within the interval [0, 1]. Therefore, the influence of g_3 factor on the estimated 3-D surface can be removed.

Fig. 6 shows a simple example of a sphere object. The first row shows a set of shadow images and the second row shows the other set of shadow images. This synthetic image was generated using the depth function of a sphere object with different light directions. So the content of the images is different. Fig. 7(a) shows the true normal vectors of the sphere. The estimated normal vectors in Fig. 7(b) and (c) were generated by using our approach corresponding to the two sets of shadow images in the first row and second row of Fig. 6. According to the estimated normal vectors in Fig. 7(b) and (c), it is obvious that the waveforms are similar to the true normal vectors. So, the estimated normal vectors do not depend on the content of the images. Furthermore, as far as the order of the sources being concerned, the similarity between human face and sphere is adopted in the supervised ICA algorithm to find the order of sources in the proposed scheme. We compute the correlation between the estimated normal vectors of surface of faces and the normal vectors of a sphere due to their similar structure, so the order of normal components can be identified.

IV. 3-D Surface Reconstruction From the Surface Normal by Enforcing Integrability

In this section, we use the enforcing integrability approach to obtain the deeper information for reconstructing of the surface of an object by its normal vectors. This approach was proposed in the earliest stage by Frankot and Chellappa in 1988 [24]. Suppose that we represent the surface $z(x, y)$ by a finite set of integrable basis functions $\phi(x, y, \boldsymbol{\omega})$ so that

$$z(x, y) = \sum_{\boldsymbol{\omega}\in\Omega} c(\boldsymbol{\omega})\phi(x, y, \boldsymbol{\omega}) \tag{32}$$

where $\boldsymbol{\omega} = (u, v)$ is a 2-D index, Ω is a finite set of indexes, and $\{\phi(x, y, \boldsymbol{\omega})\}$ is a finite set of integrable basis functions which are not necessarily mutually orthogonal. We chose the discrete cosine basis so that $\{c(\boldsymbol{\omega})\}$ is exactly the full set of discrete cosine transform (DCT) coefficients of $z(x, y)$. Since the partial derivatives of the basis functions, $\phi_x(x, y, \boldsymbol{\omega})$ and $\phi_x(x, y, \boldsymbol{\omega})$, are integrable, the partial derivatives of $z(x, y)$ are guaranteed to be integrable as well; that is, $z_{xy}(x, y) = z_{yx}(x, y)$. Note that the partial derivatives of $z(x, y)$ can also be expressed in terms of this expansion, giving

$$z_x(x, y) = \sum_{\boldsymbol{\omega}\in\Omega} c(\boldsymbol{\omega})\phi_x(x, y, \boldsymbol{\omega}) \tag{33}$$

$$z_y(x, y) = \sum_{\boldsymbol{\omega}\in\Omega} c(\boldsymbol{\omega})\phi_y(x, y, \boldsymbol{\omega}) \tag{34}$$

where $\phi_x(x, y, \boldsymbol{\omega}) = \partial\phi(\cdot)/\partial x$ and $\phi_y(x, y, \boldsymbol{\omega}) = \partial\phi(\cdot)/\partial y$.

Suppose we now have the possibly nonintegrable estimate $\mathbf{n}(x, y)$ from which we can easily deduce from (2) the possibly

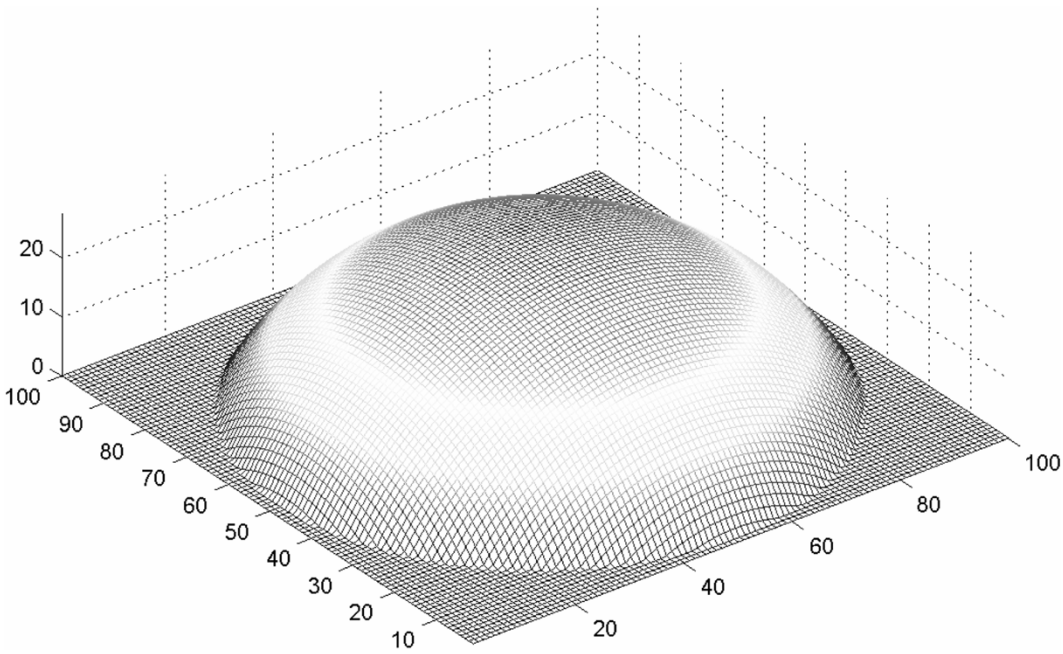

Fig. 8. Synthetic sphere surface object.

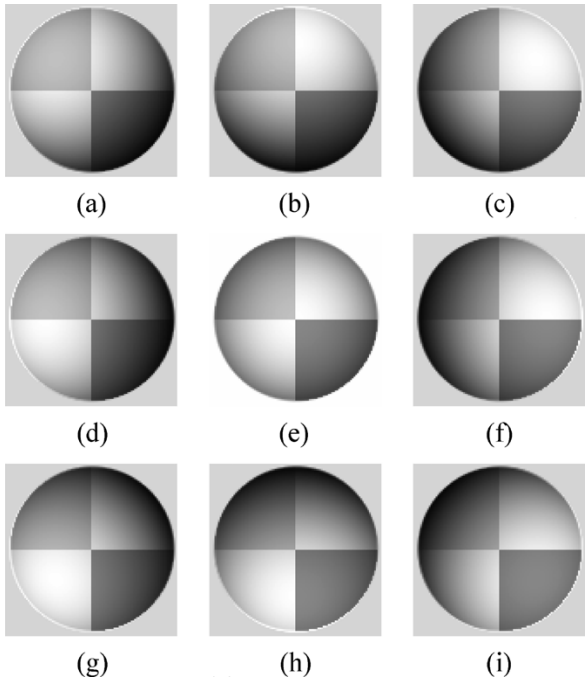

Fig. 9. The 2-D sphere images generated with varying albedo and different lighting directions (the degree of tilt angle, the degree of pan angle). (a) $S1 = (30, 140)$. (b) $S2 = (30, 90)$. (c) $S3 = (30, 40)$. (d) $S4 = (30, 180)$. (e) $S5 = (0, 0)$. (f) $S6 = (30, 0)$. (g) $S7 = (30, -140)$. (h) $S8 = (30, -90)$. (i) $S9 = (30, -40)$.

nonintegrable partial derivatives $\hat{z}_x(x, y)$ and $\hat{z}_y(x, y)$. These partial derivatives can also be expressed as a series, giving

$$\hat{z}_x(x, y) = \sum_{\boldsymbol{\omega} \in \Omega} \hat{c}_1(\boldsymbol{\omega}) \phi_x(x, y, \boldsymbol{\omega}) \tag{35}$$

$$\hat{z}_y(x, y) = \sum_{\boldsymbol{\omega} \in \Omega} \hat{c}_2(\boldsymbol{\omega}) \phi_y(x, y, \boldsymbol{\omega}). \tag{36}$$

TABLE I
THE ABSOLUTE MEAN ERRORS BETWEEN ESTIMATED DEPTHS AND DESIRED DEPTH OF SYNTHETIC OBJECT'S 3-D SURFACES. (BOTH LIGHT AND VIEWING DIRECTIONS ARE UNKNOWN IN THE EXPERIMENT)

Mean absolute depth error	Lights	Georghiades's method ([11])	Hayakawa's method ([20])	Our proposed method
Sphere with Variant albedo	S1, S2, S3	0.048875	0.07688	0.02025
	S7, S8, S9	0.050316	0.07924	0.02687
	S1, S5, S3	0.033133	0.07279	0.02055
	S1, S8, S6	0.033529	0.07869	0.01837
	S1, S5, S7	0.031729	0.07621	0.01829

A method has been proposed for finding the expansion coefficients $c(\boldsymbol{\omega})$ given a possibly nonintegrable estimate of surface slopes $\hat{z}_x(x, y)$ and $\hat{z}_y(x, y)$

$$c(\boldsymbol{\omega}) = \frac{p_x(\boldsymbol{\omega}) \hat{c}_1(\boldsymbol{\omega}) + p_y(\boldsymbol{\omega}) \hat{c}_2(\boldsymbol{\omega})}{p_x(\boldsymbol{\omega}) + p_y(\boldsymbol{\omega})}, \text{ for } \boldsymbol{\omega} = (u, v) \in \Omega \tag{37}$$

where $p_x(\boldsymbol{\omega}) = \int\int |\phi_x(x, y, \boldsymbol{\omega})|^2 dxdy$ and $p_y(\boldsymbol{\omega}) = \int\int |\phi_y(x, y, \boldsymbol{\omega})|^2 dxdy$. Finally, we can reconstruct the object's surface by performing the inverse 2-D DCT on the coefficients $c(\boldsymbol{\omega})$.

V. EXPERIMENTAL RESULTS AND DISCUSSIONS

In this section, two experiments are performed to assess the performance of the proposed approach. In the first experiment, we test the algorithm on synthetically generated images for the reconstruction of surface of objects. The light direction and viewing direction are unknown. In the second experiment, we test the algorithm on a number of real images captured from the Yale Face Database B [34] showing the variability due to illumination and there is varying albedo in each point of surface of human faces. All the experimental results are compared to those of the Georghiades's approach in [11] and the Hayakawa's approach in [20] tested on the same images.

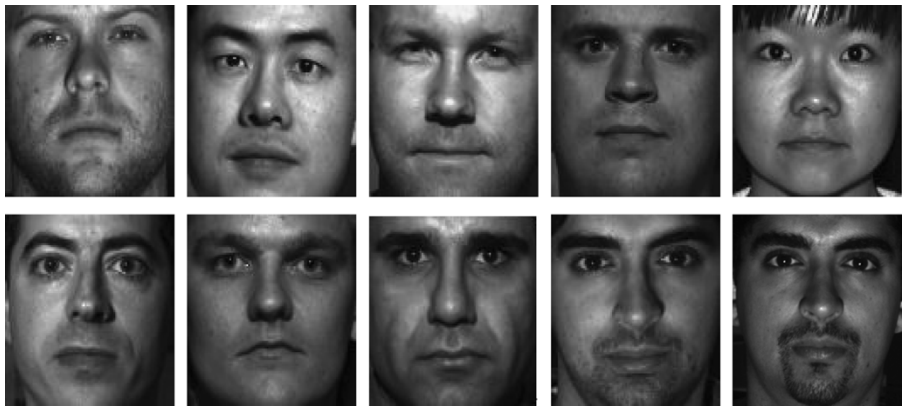

Fig. 10. 10 individuals from the Yale face database B used to test our algorithm.

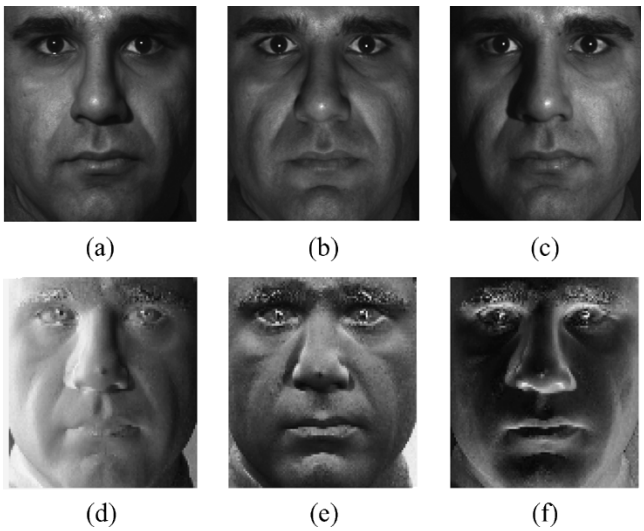

Fig. 11. Three training images with differ light source positions from Yale Face Database B in frontal. (b) Surface normal corresponding to the three source images.

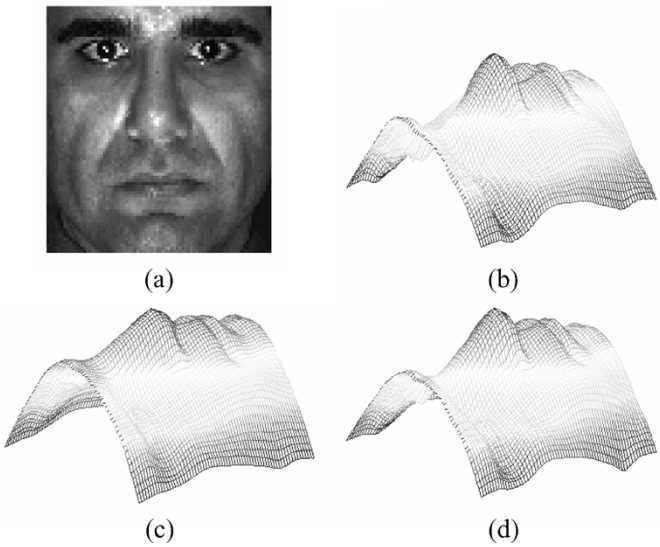

Fig. 12. The surface albedo of human face in Fig. 11. The results of 3-D model reconstruction by (b) our proposed algorithm, (c) Georghiades's approach in [11], and (d) Hayakawa's approach in [20].

A. Quantitative Experimental Results by Reconstructing a Synthetic Sphere Object

Quantitative experimental results have been obtained by reconstructing a synthetic sphere object. The true depth map of the synthetic sphere object is generated mathematically as

$$z(x,y) = \begin{cases} |\sqrt{r^2 - x^2 - y^2}|, & \text{if } x^2 + y^2 \leq r^2 \\ 0, & \text{otherwise} \end{cases} \quad (38)$$

where $r = 48$, $0 < x, y \leq 100$, and the center is located at $(x, y) = (51, 51)$. The sphere object is showed in Fig. 8. This synthetic image was generated using the depth function in (38) and the surface gradients were computed using the discrete approximation. Fig. 9 shows the synthetic images generated according to the non-Lambertian model with varying albedo and different directions. The different albedos are, 0.6 for right-bottom of the sphere, 0.8 for left-top of the sphere, and 1 for the rest part. The locations of light sources in Figs. 9(a)–(i) are $\mathrm{S1} = (30, 140)$, $\mathrm{S2} = (30, 90)$, $\mathrm{S3} = (30, 40)$, $\mathrm{S4} = (30, 180)$, $\mathrm{S5} = (0, 0)$, $\mathrm{S6} = (30, 0)$, $\mathrm{S7} = (30, -140)$, $\mathrm{S8} = (30, -90)$, and $\mathrm{S9} = (30, -40)$, where the first component is the degree of tilt angle and the second component is the degree of pan angle. The center of image is set as the origin of the coordination. The x-y plane is parallel to the image plane. The z-axis is perpendicular to the image plane. The experimental results are shown in Table I and the proposed method is compared with two photometric stereo algorithms, Hayakawa's method and Georghiades's method. In Table I, we take five groups of images with different illuminant angles from the left, the right, and the front for 3-D reconstruction. Both estimated surface and synthetic one are normalized within the interval [0, 1]. According to Table I, it is found that the proposed method can achieve the lowest mean errors compared with the other methods in all illumination conditions.

B. Experimental Results on Real Images With Varying Albedo

In the second experiment, we test the algorithm on a number of real images from the Yale Face Database B [34] showing the variability due to illumination and there is varying albedo in each point of surface of human faces. This subset contains 444 viewing conditions (1 pose $\times$ 37 illumination conditions, where these illumination conditions contain Subset1 (12°) and Subset2 (25°) in the Yale Face Database B.) for 10 individuals. Fig. 10 shows the 10 individuals from the Yale Face Database B

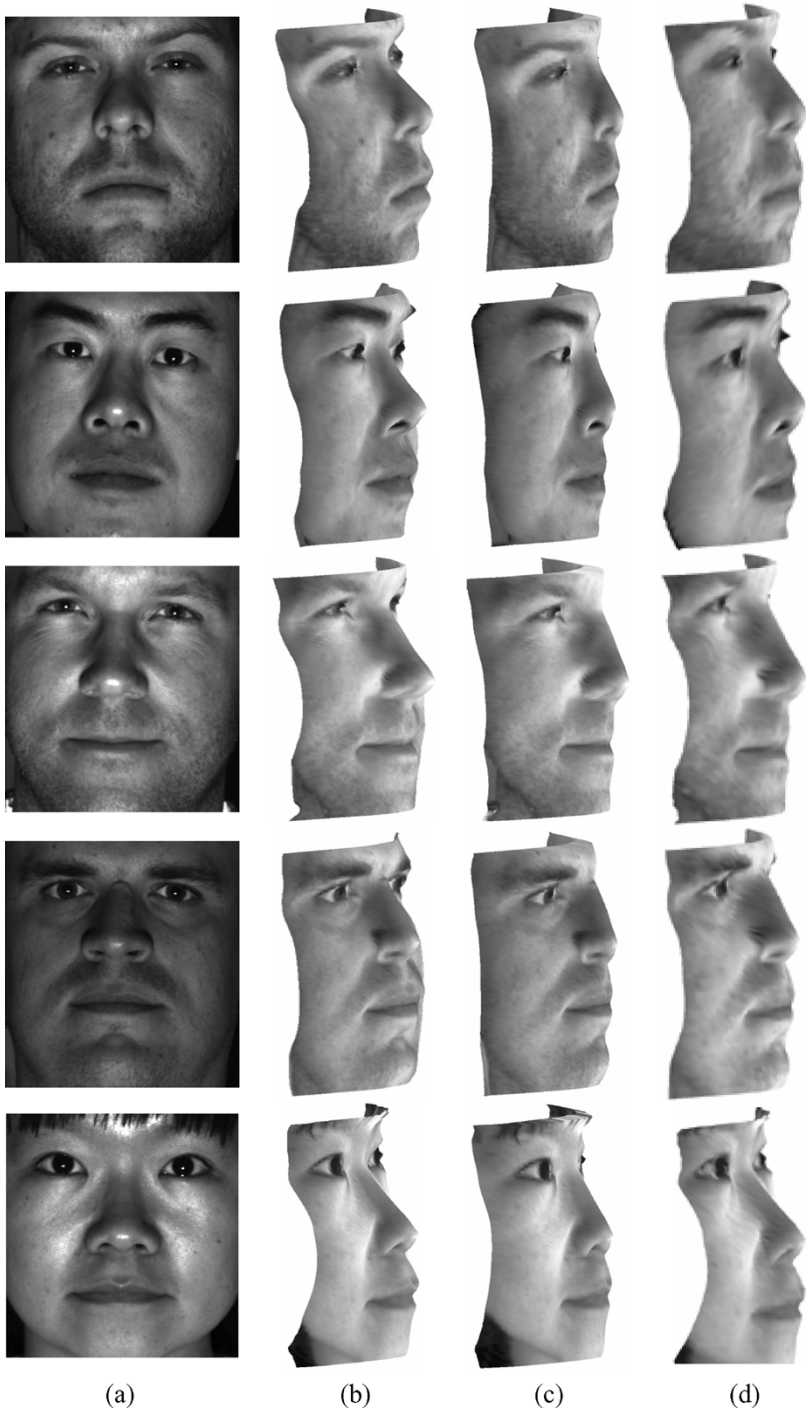

Fig. 13. The results of 3-D model reconstruction by (b) our proposed algorithm, (c) Georghiades's approach in [11], and (d) Hayakawa's approach in [20].

used to test our algorithm, where each image size is 100×100 in pixels.

First, we take the images of the same person that was photographed under three different light sources from these testing images arbitrarily shown in Fig. 11. We feed the normalized images into our algorithm. After updating the parameters by several iterations, we can get the normal vector of the surfaces of human faces corresponding to each pixel in an image in the output nodes. The results are shown in the second row in Fig. 11, which are the first component, the second component, and the third component of the surface normal vector in order. Fig. 12 presents the results of 3-D human face reconstruction. Fig. 12(a) shows the surface albedo of human face in Fig. 11. Fig. 12(b) shows the result with our proposed algorithm. By using the Georghiades's approach [11] and the Hayakawa's approach [20], the reconstructed results are demonstrated in Fig. 12(c) and (d), respectively. The results clearly indicate that the performance of our proposed nonlinear reflectance model is better than that of the Georghiades's approach and the Hayakawa's approach. Comparing to the results obtained by the Georghiades's approach, the reconstructed surfaces with the consideration of specular components in our algorithm,

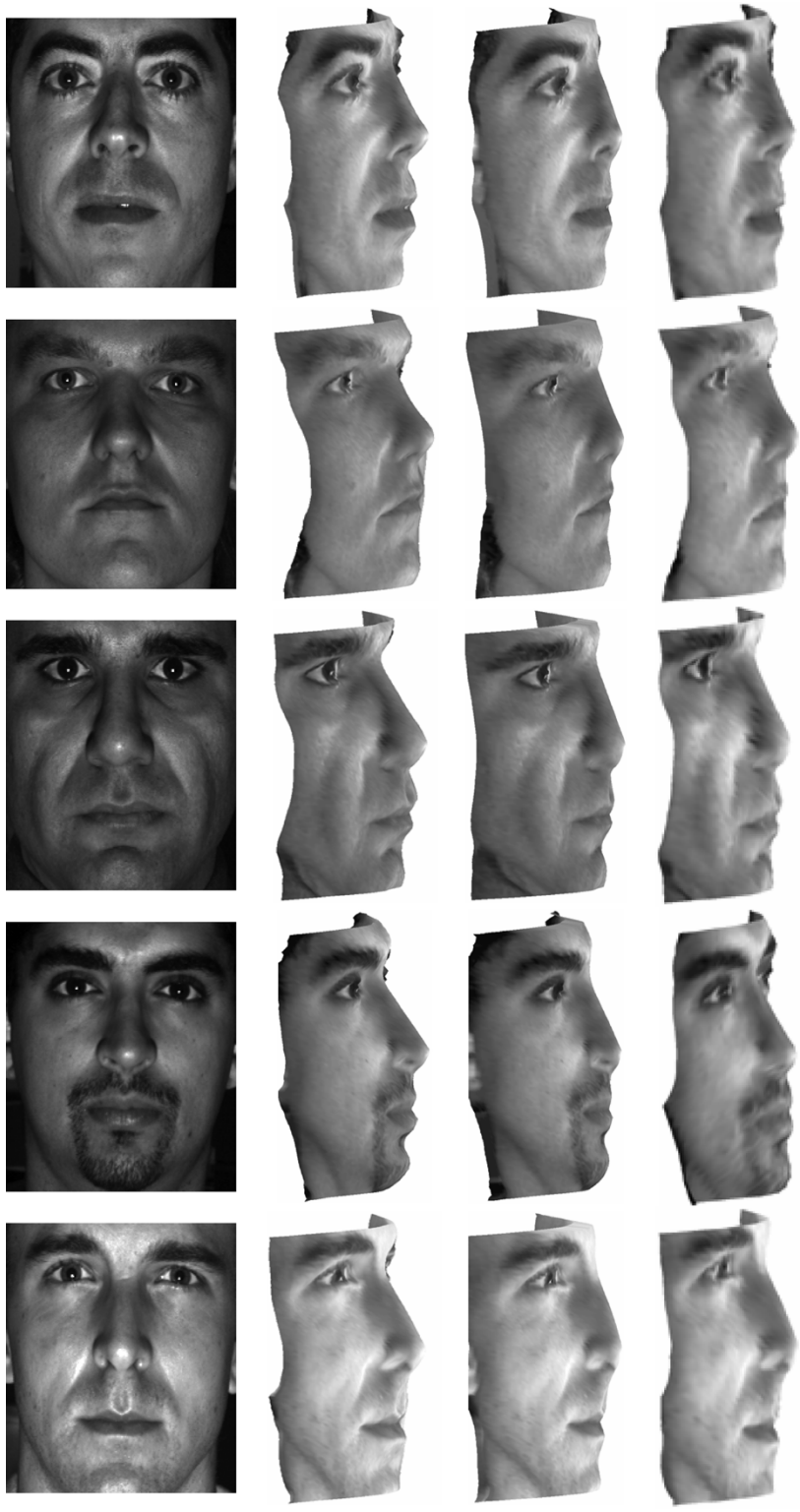

Fig. 14. The results of 3-D model reconstruction by (b) our proposed algorithm, (c) Georghiades's approach in [11], and (d) Hayakawa's approach in [20].

are obviously better in high-gradient parts such as the nose. Besides, the Hayakawa's approach did need added constraints, it could reconstruct the 3-D model of human face similar as our approach, but when the constraints is unavailable, then it could not reconstruct the 3-D model of human face. Finally, the reconstructed results for the testing patterns are shown in Fig. 13 and Fig. 14.

VI. Conclusions

It has been claimed that methods based on reconstructing 3-D face model for face recognition are quite successful. When we are estimating the surface shape, the success of the reflectance model for surface reconstruction of objects depends on two major components: the diffuse component and the specular

component. Therefore, in this paper, we proposed a new nonlinear reflection model consisting of the diffuse components and the specular components. The past researches only considered the linear combination of the diffuse components and the specular components. We do not need to separate the two components in the proposed novel nonlinear reflection model. In addition to this major contribution, several contributions of the proposed algorithm are listed.

1) In the past, we have to know the locations of light sources first for solving the photometric stereo problems. But this is not practical in the real situations. In this paper, we used the images under three different light source locations to solve this problem. In our method, we can still obtain a very good result even if the locations of light sources are not given.
2) Using the unsupervised nonlinear ICA network for solving photometric stereo problems does not need any desired output value and the smoothing conditions. It is easier to converge and make the system stable.

The performance comparisons of our proposed nonlinear reflectance model to the Georghiades's approach in [11] and the Hayakawa's approach in [20] were made. In the first experiment, we test the algorithm on synthetically generated images for the reconstruction of surface of objects. The results clearly indicate that the performances of our proposed nonlinear reflectance model are better than that of the Georghiades's approach in [11] and the Hayakawa's approach in [20]. In the second experiment, we test the algorithm on a number of real images from the Yale Face Database B containing the variability due to illumination and varying albedo in each point of surface of human faces. All the experimental results showed that the performance of the proposed nonlinear reflectance model is better than those of the two proposed existing photometric stereo methods.

REFERENCES

[1] K. P. Horn, "Shape from shading: a smooth opaque object from one view," Ph. D. dissertation, Mass. Inst. Technol., Cambridge, 1970.

[2] R. J. Woodham, "Photometric method for determining surface orientation from multiple images," *J. Opt. Eng.*, vol. 19, no. 1, 1980.

[3] K. M. Lee and C. C. J. Kuo, "Shape reconstruction from photometric stereo," *J. Opt. Soc. Amer.: A*, vol. 10, no. 5, 1993.

[4] C. Cho and H. Minanitani, "A new photometric method using 3 point light sources," *IEICE Trans. Inform. Syst.*, vol. V.E76-D, no. 8, pp. 898–904, Aug. 1993.

[5] Y. Iwahori, R. Woodham, and A. Bagheri, "Principal components analysis and neural network implementation of photometric stereo," in *Proc. Workshop on Physics-Based Modeling in Computer Vision*, Jun. 1995, pp. 117–125.

[6] G. Kay and T. Caelli, "Estimating the parameters of an illumination model using photometric stereo," *Graphical Models and Image Process.*, vol. 57, no. 5, pp. 365–388, 1995.

[7] G. McGunnigle, "The classification of textured surfaces under varying illuminant direction," Ph.D. dissertation, Dep. Computing and Elect. Eng., Heriot-Watt Univ., Edinburgh, Scotland, 1998.

[8] S. K. Nayar, K. Ikeuchi, and T. Kanade, "Determining shape and reflectance of hybrid surfaces by photometric sampling," *IEEE Trans. Robot. Autom.*, vol. 6, no. 4, pp. 418–431, 1990.

[9] E. Angelopoulou and J. P. Williams, "Photometric surface analysis in a triluminal environment," in *Proc. IEEE Int. Conf. Computer Vision*, 1999.

[10] P. N. Belhumeur, D. J. Kriegman, and A. L. Yuille, "The Bas-belief ambiguity," *CVPR*, pp. 1060–1066, 1997.

[11] S. Georghiades, P. N. Belhumeur, and D. J. Kriegman, "From few to many: illumination cone models for face recognition under variable lighting and pose," *IEEE Trans. Pattern Anal. Machine Intell.*, vol. 23, no. 6, pp. 643–660, Jun. 2001.

[12] S. Georghiades, "Incorporating the torrance and sparrow model of reflectance in uncalibrated photometric stereo," in *Proc. 9th IEEE Int. Conf. Computer Vision*, 2003.

[13] K. Ikeuchi, "Determining surface orientations of specular surfaces by using the photometric stereo method," *IEEE Trans. Pattern Anal. Machine Intell.*, vol. 3, pp. 661–669, 1981.

[14] E. N. Coleman and R. Jain, "Obtaining 3Dimensional shape of textured and specular surfaces using four-source photometry," *Process. Computer Vision, Graphics, and Image*, vol. 18, pp. 309–328, 1982.

[15] H. D. Tagare and R. J. P. deFigueiredo, "Simulataeous estimation of shape and reflectance maps from photometric stereo," in *IEEE Int. Conf. Comput. Vision*, 1990, pp. 340–343.

[16] F. Solomon and K. Ikeuchi, "Extracting the shape and roughness of specular lobe objects using four light photometric stereo," *IEEE Conf. Comput. Vision and Pattern Recogn.*, pp. 466–471, 1992.

[17] H. Rushmeier, G. Taubin, and A. Gueziec, "Applying shape from lighting variation to bump map capture," in *In Eurographics Rendering Tech. '97*, St. Etienne, France, June 1997, pp. 35–44.

[18] O. Drbohlav and A. Leonardis, "Detecting shadows and specularities by moving light," in *Proc. Computer Vision Winter Workshop*, Ljubljana, Slovenia, 1998, pp. 60–74.

[19] O. Drbohlav and R. Sara, "Specularities reduce ambiguity of uncalibrated photometric stereo," in *Proc. 7th Europ. Conf. Computer Vision*, Copenhagen, Denmark, 2002.

[20] K. Hayakawa, "Photometric stereo under a light source with arbitrary motion," *J. Opt. Soc. Amer.: A*, vol. 11, no. 11, 1994.

[21] H. Wang, Y. Wang, and H. Wei, "Face representation and reconstruction under different illumination conditions," in *Proc. 7th Int. Conf. Information Visualization*, 2003.

[22] A. Taleb and C. Jutten, "Nonlinear source separation: the post-nonlinear mixtures," in *Proc. ESANN*, Bruges, Belgium, 1997, pp. 279–284.

[23] ——, "Source separation in post-nonlinear mixtures," *IEEE Trans. Signal Process.*, vol. 47, no. 10, pp. 2807–2820, Oct. 1999.

[24] R. T. Frankot and R. Chellappa, "A method for enforcing integrability in shape from shading algorithms," *IEEE Trans. Pattern Anal. Machine Intell.*, vol. 10, no. 4, pp. 439–451, Jul. 1988.

[25] R. Bell and T. J. Sejnowski, "An information-maximization approach to blind separation and blind deconvolution," *Neural Comput.*, vol. 7, pp. 1129–1159, 1995.

[26] S. I. Amari, "Natural gradient works efficiently in learning," *Neural Comput.*, vol. 10, pp. 251–276, 1998.

[27] A. Hyvärinen, J. Karhunen, and E. Oja, *Independent Component Analysis*. New York: Wiley, 2001.

[28] M. D. Plumbley, "Algorithms for nonnegative independent component analysis," *IEEE Trans. Neural Netw.*, vol. 14, no. 3, pp. 534–543, May 2003.

[29] M. D. Plumbley and E. Oja, "A "nonnegative PCA" algorithm for independent component analysis," *IEEE Trans. Neural Netw.*, vol. 15, no. 1, pp. 66–76, Jan. 2004.

[30] D. Martinez and A. Bray, "Nonlinear blind source separation using kernels," *IEEE Trans. Neural Netw.*, vol. 14, no. 1, pp. 228–235, Jan. 2003.

[31] F. Acernese, A. Ciaramella, S. De Martino, R. De Rosa, M. Falanga, and R. Tagliaferri, "Neural networks for blind-source separation of Stromboli explosion quakes," *IEEE Trans. Neural Netw.*, vol. 14, no. 1, pp. 167–175, Jan. 2003.

[32] L. Zhang, A. Cichocki, and S. Amari, "Self-adaptive blind source separation based on activation functions adaptation," *IEEE Trans. Neural Netw.*, vol. 15, no. 2, pp. 233–244, Mar. 2004.

[33] S. A. Cruces-Alvarez, A. Cichocki, and S. Amari, "From blind signal extraction to blind instantaneous signal separation: criteria, algorithms, and stability," *IEEE Trans. Neural Netw.*, vol. 15, no. 4, pp. 859–873, Jul. 2004.

[34] *http://cvc.yale.edu/projects/yalefacesB/yalefacesB.html* [Online]

Chin-Teng (CT) Lin (F'05) received the B.S. degree from National Chiao-Tung University (NCTU), Taiwan, in 1986, and the Ph.D. degree in electrical engineering from Purdue University, West Lafayette, IN, in 1992.

He is currently the Chair Professor of Electrical and Control Engineering, Dean of Computer Science College, and Director of Brain Research Center at NCTU. He was Director of the Research and Development Office of NCTU from 1998 to 2000, Chairman of Electrical and Control Engineering Department of NCTU from 2000 to 2003, and Associate Dean of the College of Electrical Engineering and Computer Science from 2003 to 2005. His current research interests are fuzzy neural networks, neural networks, fuzzy systems, cellular neural networks, neural engineering, algorithms and VLSI design for pattern recognition, intelligent control and multimedia (including image/video and speech/audio) signal processing, and intelligent transportation system (ITS). He is the coauthor of *Neural Fuzzy Systems—A Neuro-Fuzzy Synergism to Intelligent Systems* (Englewood Cliffs, NJ: Prentice Hall, 1996) and the author of *Neural Fuzzy Control Systems with Structure and Parameter Learning* (New York: World Scientific, 1994). He has published more than 90 journal papers in the areas of neural networks, fuzzy systems, multimedia hardware/software, and soft computing, including about 60 IEEE JOURNAL papers.

Dr. Lin was elected the IEEE Fellow for his contributions to biologically inspired information systems. He is a Member of Tau Beta Pi, Eta Kappa Nu, and Phi Kappa Phi. He is on Board of Governors of the IEEE Circuits and Systems (CAS) Society for 2005 and IEEE Systems, Man, Cybernetics (SMC) Society for 2003–2005. He is the Distinguished Lecturer of the IEEE CAS Society for 2003 to 2005. He is the International Liaison of the International Symposium of Circuits and Systems (ISCAS) 2005 in Japan, Special Session Cochair of ISCAS 2006 in Greece, and the Program Cochair of the IEEE International Conference on SMC 2006, in Taiwan. He has been the President of the Asia Pacific Neural Network Assembly since 2004. He received the Outstanding Research Award from the National Science Council, Taiwan, from 1997 to present, the Outstanding Electrical Engineering Professor Award from the Chinese Institute of Electrical Engineering (CIEE) in 1997, the Outstanding Engineering Professor Award from the Chinese Institute of Engineering (CIE) in 2000, and the 2002 Taiwan Outstanding Information-Technology Expert Award. He was elected to be one of the*38th Ten Outstanding Rising Stars in Taiwan* (2000). He is an Associate Editor of IEEE TRANSACTIONS ON CIRCUITS AND SYSTEMS, PART I and PART II, IEEE TRANSACTIONS ON SYSTEMS, MAN, AND CYBERNETICS, and IEEE TRANSACTIONS ON FUZZY SYSTEMS and *International Journal of Speech Technology*.

Wen-Chang Cheng received the B.S. degree in electrical engineering from National Cheng-Kung University (NCKU), Tainan, Taiwan, the M.S. degree in electrical engineering from National Chung-Cheng University (CCU), Chiayi, Taiwan, in 1997 and 1999, respectively. He received the Ph.D. degree in electrical and control engineering from the National Chiao-Tung University (NCTU), Hsinchu, Taiwan, in 2005.

Currently, he is an Assistant Professor of the Information Networking Technology Department, Hsiuping Institute of Technology, Taichung, Taiwan. His current research interests include neural networks, fuzzy systems, neurofuzzy systems, image processing, machine learning, artificial intelligence, and intelligent transportation system (ITS).

Sheng-Fu Liang was born in Tainan, Taiwan, in 1971. He received the B.S. and M.S. degrees in control engineering from the National Chiao-Tung University (NCTU), Hsinchu, Taiwan, in 1994 and 1996, respectively. He received the Ph.D. degree in electrical and control engineering from NCTU in 2000.

From 2001 to 2005, he was a Research Assistant Professor in the Electrical and Control Engineering Department, NCTU. In 2005, he joined the Department of Biological Science and Technology, NCTU, where he serves as an Assistant Professor. He has also served as the chief executive of Brain Research Center, NCTU Branch, University System of Taiwan, since September 2003. His current research interests are biomedical engineering, biomedical signal/image processing, machine learning, fuzzy neural networks (FNN), the development of brain-computer interface (BCI), and multimedia signal processing.